euronoise

Investigation of 3-D benchmark problems in underwater acoustics: a uniform approach

Frederic Sturm

Laboratoire de Mécanique des Fluides et d'Acoustique (UMR CNRS 5509), Ecole Centrale de Lyon, Centre acoustique, 36, avenue Guy de Collongue, 69134 Ecully Cedex, France
frederic.sturm@ec-lyon.fr

In this paper, we report numerical results corresponding to the propagation of broadband pulses in the several three-dimensional oceanic benchmarks: the wedge-shaped waveguide, the gaussian canyon, and the sinusoidal bottom. The objective is to propose a uniform representation of the numerical results so as to facilitate the comparison of the 3-D effects present in each benchmark. The originality of the current work is to systematically present snapshots of the propagating pulses at very close successive times. The numerical simulations are performed using a fully 3-D parabolic equation based model coupled with a Fourier synthesis technique to handle the time dependence of the source signal.

1 Introduction

In underwater acoustics, most of the three-dimensional (3-D) effects on sound wave propagation are usually described by modelers considering one of the following shallow-water benchmark problems: a wedge-shaped waveguide, a gaussian canyon, a conical seamount, and a sinusoidal bottom (see for instance in Ref. [1]). These test cases have been thoroughly analyzed individually considering both harmonic point sources (emitting at very low frequencies, for some obvious problems of both CPU time and memory limitation) and broadband source pulses (with also very low center frequencies). In the present work, we report numerical results corresponding to the propagation of broadband pulses in three of the four above-mentioned test cases. The objective is to propose a uniform representation of the numerical results so as to facilitate the comparison of the 3-D effects. To that end, snapshots of the propagating pulses at very close successive times are shown, analyzed, and compared with 2-D results. Along with the snapshots come movies [2] shown during the oral presentation. Snapshots and movies strongly facilitate the observation and thus the understanding of the 3-D effects experienced by the propagating waves.

2 Description of the test cases

We consider three acoustic problems well known in the underwater acoustics community as the 3-D wedge [3], [4] (three-dimensional extension of the original 2-D ASA wedge benchmark), the 3-D gaussian canyon (variant of the test case devised for the SWAM'99 workshop [5]), and the sinusoidal (corrugated) bottom originally proposed by Collins and Chin-Bing [6]. In this paper, we will refer to these three problems as test cases A, B, C, respectively. All of them involve an acoustic point source placed in an oceanic environment which consists of a lossless homogeneous water layer with a sound speed of 1500 m/s and a density of 1 g/cm^3, overlying a lossy half-space sediment bottom with a sound speed of 1700 m/s, a density of 1.5 g/cm^3, and an aborption of 0.5 dB per wavelength. The three test cases considered here differ in the description of the bottom geometry. The water/sediment interface is described by the surface $\{z = h(r, \theta)\}$ where

$$h(r,\theta) = 200\left(1 - \frac{r\cos\theta}{4000}\right), \qquad \text{(test case A)}$$

$$h(r,\theta) = 20 + 180\exp\left[-\left(\frac{r\cos\theta}{720}\right)^2\right], \qquad \text{(test case B)}$$

$$h(r,\theta) = 150 - 50\sin\left(\frac{2\pi r\cos\theta}{6000}\right). \qquad \text{(test case C)}$$

For test case A, the water/sediment interface makes an angle of 2.86° with respect to the ocean surface at both $\theta = 0°$ (upslope direction) and and $\theta = 180°$ (downslope direction) and is invariant along the azimuth $\theta = 90°$. For test case B, the interface describes a gaussian curve, with a maximum slope value of approximately 12.1° at 509 m along the $\theta = 0°$ and $\theta = 180°$ upslope directions. Like test case A, the interface is characterized by a zero-slope at $\theta = 90°$. For test case C, the interface is a sinusoid of 6000-m periodicity for the particular azimuthal angles $\theta = 0°$ and $\theta = 180°$. Again, the bottom is flat for $\theta = 90°$. The acoustic point source is placed at $r = 0$ at a depth of 40 m for test cases A, B, and 25 m for test case C. The source signal is a gaussian-weighted cosine pulse given by $\mathcal{S}(t) = \cos(2\pi f_c t)\,\exp\left[-(5\pi t)^2\right]$ with center frequency $f_c = 25$ Hz. Note that the water depth at the source location is 200 m for test cases A, B, and 150 m for test case C.

The numerical simulations presented in the following sections were performed using the 3-D parabolic equation based model 3DWAPE [7] coupled with a Fourier synthesis technique to handle the time dependence of the source signal.

3 Results for test case A

For test case A, images of transmission loss corresponding to fully 3-D computations at 25 Hz are shown in Fig. 1 for two specific azimuthal directions. Previous

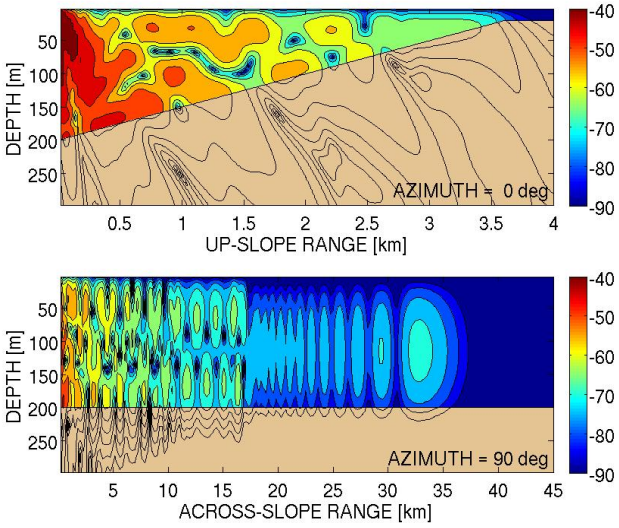

Figure 1: Transmission loss (in dB re 1 m) at 25 Hz for test case A corresponding to 3-D PE computations. Vertical slices at $\theta = 0°$ (upper plot, $r_{\max} = 4$ km) and $\theta = 90°$ (lower plot, $r_{\max} = 45$ km).

studies showed that there is no 3-D effects along the

up-slope direction ($\theta = 0°$). However, remarkable 3-D effects can be observed in the cross-slope direction ($\theta = 90°$). Those effects have been explained in detail by several authors (see for instance in Ref. [8]) and correspond to intramodal interference effects, leading to a succession of distinct zones across slope, with three propagating modes in the first zone, two propagating modes in the second zone, one propagating mode (clearly interfering with itself) in the third zone, followed by a shadow zone. Note that numerical solutions for this 3-D problem are generally presented considering a maximum computation range $r_{\max}$ of 25 km [9]. Here, in order to catch the shadow zone of mode 1, the value of $r_{\max}$ has been increased to 45 km.

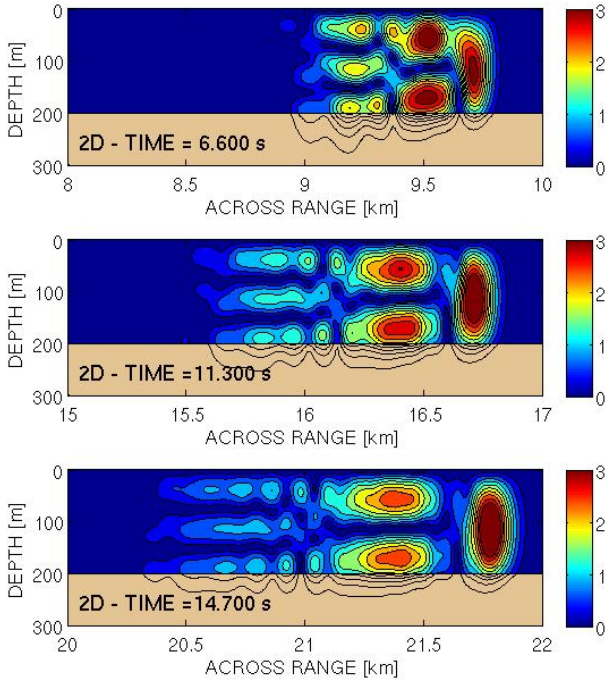

Figure 2: Snapshots of the envelop of the propagating pulse along the $\theta = 90°$ azimuthal direction for test case A corresponding to 2-D PE computations.

Snapshots of the propagating pulses at several discrete times are shown in Fig. 2 (2-D computations) and in Fig. 3 (3-D computations). Note that both 2-D and 3-D solutions were multiplied by a factor r to compensate for spherical spreading. As can be seen in Fig. 2, a zero-slope bathymetry shows the presence, on each snapshot displayed, of three distinct wave packets more and more dispersed as time increases, corresponding to the signals carried by the three propagating modes. Now, looking at Fig. 3, due to the 2.86°-wedge bathymetry, the three modes are horizontally refracted down the slope, leading to several typical 3-D effects easily identifiable on each snapshot. Note that at short range, the 3-D effects are rather weak. This explains the presence of the three propagating modes in the 3-D solution at $t = 6.6$ s. Then we observe successively the following features: extinction of mode 3 (*cf.* $t = 10$ s), extinction of mode 2 (*cf.* $t = 13.3$ s) preceded by a stronger and more dispersed mode-2 arrival at $t = 11.3$ s (this effect corresponds to the merger of two distinct time arrivals of mode 2), two distinguishable mode-1 arrivals at $t \geq 14.7$ s (note that a discerning look at $t = 13.3$ s

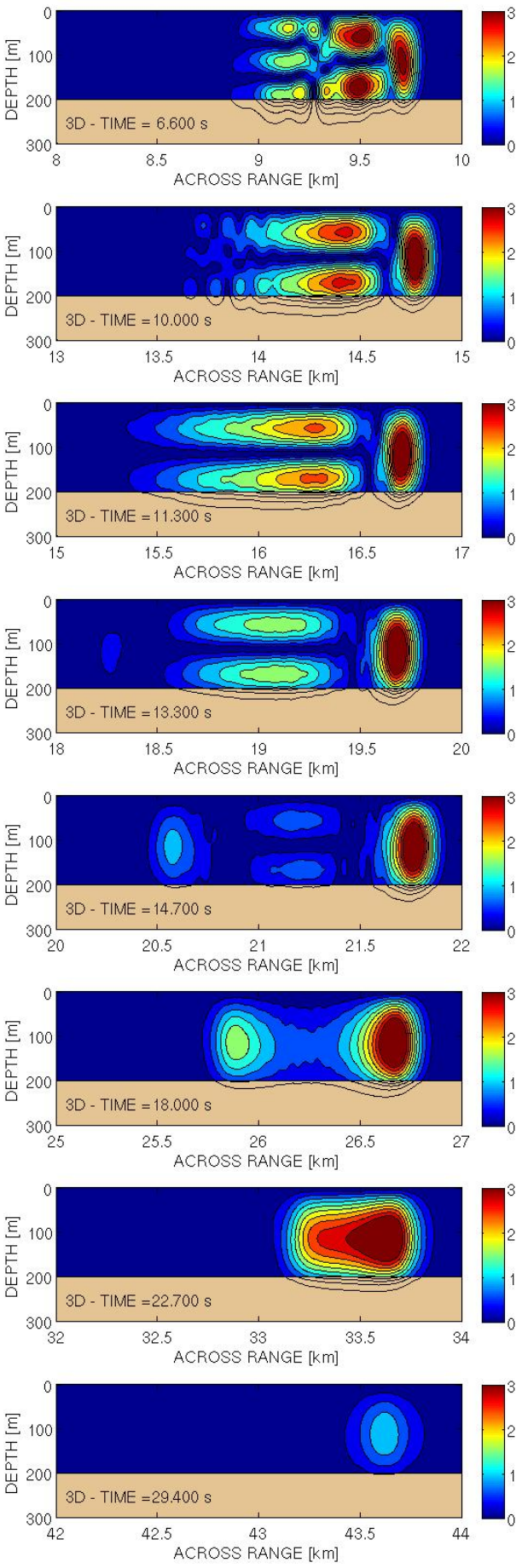

Figure 3: Snapshots of the envelop of the propagating pulse along the $\theta = 90°$ azimuthal direction for test case A corresponding to fully 3-D PE computations.

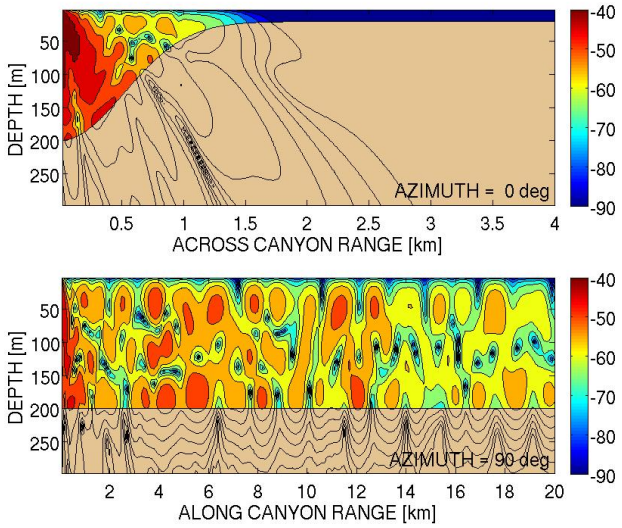

Figure 4: Transmission loss (in dB re 1 m) at 25 Hz for test case B corresponding to 3-D PE computations. Vertical slices at $\theta = 0°$ (upper plot, $r_{\max} = 4$ km) and $\theta = 90°$ (lower plot, $r_{\max} = 20$ km).

reveals the presence, though very weak, of the second arrival of mode 1), and mode-1 extinction (*cf.* $t = 29.4$ s). It should be noted that like mode 2, the extinction of mode 1 is preceded by a strong mode-1 arrival corresponding to the merger of the first and second arrivals of mode 1 (*cf.* $t = 22.7$ s).

4 Results for test case B

For test case B, images of transmission loss at 25 Hz are displayed in Fig. 4 and snapshots of the propagating pulses are shown in Fig. 5 (3-D computations). Note that the snapshots corresponding to 2-D computations are rigorously similar to the ones shown in Fig. 2. For this second test case, the acoustic energy is horizontally refracted by the sidewalls of the gaussian canyon and channeled along the canyon axis. As a consequence, due to the focusing of the energy along the canyon axis, the amplitude of the 3-D solution along the azimuth $\theta = 90°$ is considerably higher than that of the 2-D solution along the same azimuth (compare the scaling used in Fig. 5 with the one used in Fig. 2). The differences between 2-D and 3-D solutions are enhanced by the fact that the sound source is placed midway across the canyon.

The snapshots show that the modal structure of the propagating pulses gets more and more complicated as t increases. This is due to the fact that the focusing of the energy along the canyon axis is repetitive in range for each propagating mode and more pronounced for higher modes than for lower modes. For instance, the repetitivity of mode 3 can be observed on the snapshots at $t = 3.3$ s, $t = 6.3$ s, $t = 10$ s, and the repetitivity of mode 2 can be observed at $t = 4.7$ s, $t = 8.3$ s, $t = 12$ s. Besides, the presence of multiple arrivals (separated in time) for each of the three propagating modes can be observed (*e.g.* several mode-2 arrivals at $t = 12$ s and several mode-3 arrivals at $t = 13.4$ s). Note that the maximum slope of the bathymetry in the

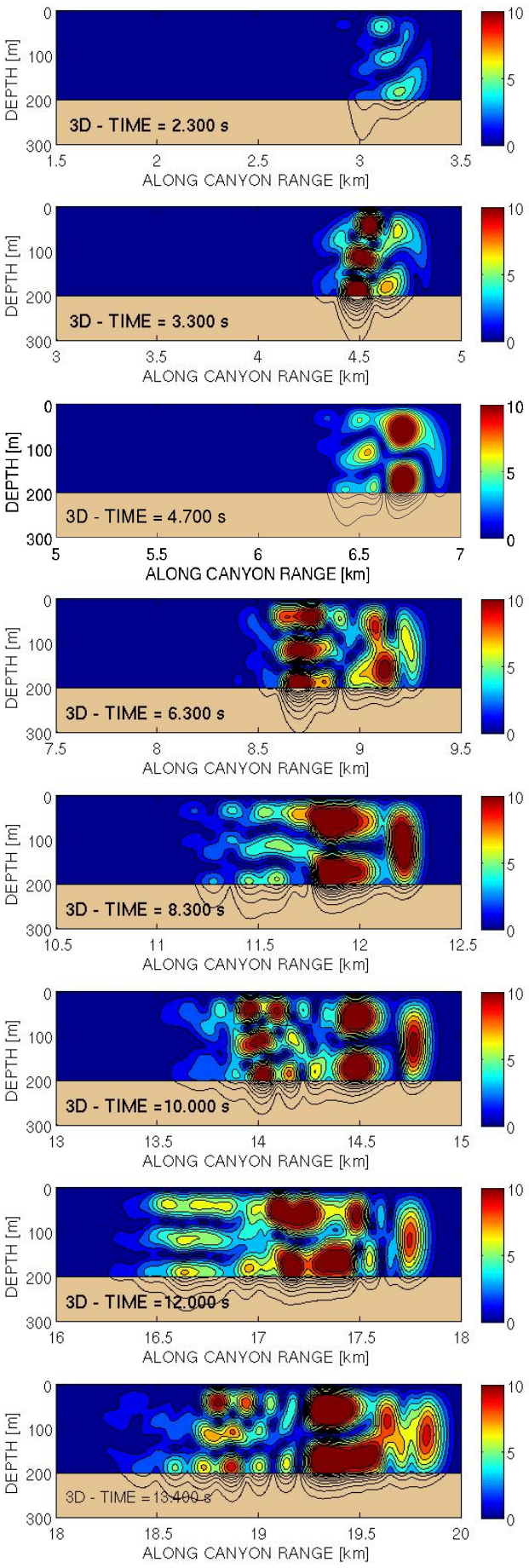

Figure 5: Snapshots of the envelop of the propagating pulse along the $\theta = 90°$ azimuthal direction for test case B corresponding to fully 3-D PE computations.

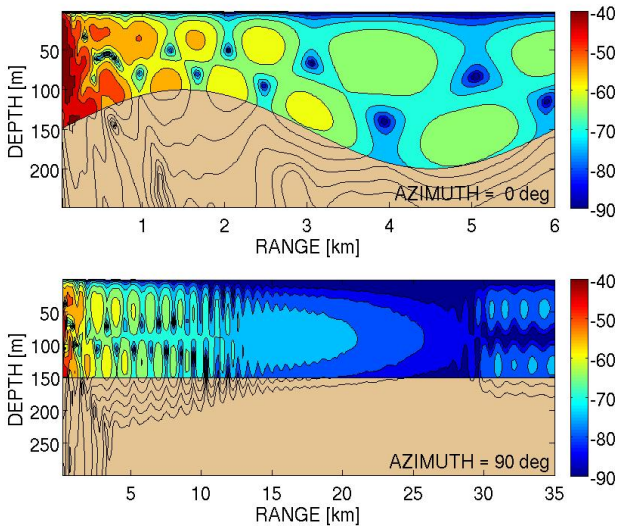

Figure 6: Transmission loss (in dB re 1 m) at 25 Hz for test case C corresponding to 3-D PE computations. Vertical slices at $\theta = 0°$ (upper plot, $r_{\max} = 6$ km) and $\theta = 90°$ (lower plot, $r_{\max} = 35$ km).

cross-canyon direction is much larger than the 2.86°-slope of test case A. The 3-D effects are accordingly detectable sooner in range and are more marked than for test case A. Note that, in addition, unlike test case A, no shadow zone is observed along the canyon axis.

5 Results for test case C

For test case C, vertical slices of the transmission loss are shown in Fig. 6. Snapshots are displayed in Fig. 7 (2-D computations) and in Fig. 8 (3-D computations). For this third test case, previous works showed that the main 3-D effects are located along the channel axis and at long ranges [6], [10]. As in test case B, this is due to the fact that, during its propagation, the acoustical energy is horizontally refracted by the sidewalls of the sinusoidal bottom, thus trapped in the deeper part of the waveguide, and channeled along the $\theta = 90°$ azimuthal direction. Note however that unlike test case B, the sound source is not placed above the deeper part of the waveguide, thus shifting the high-intensity caustic zones of the 3-D effects. Besides, the maximum slope (approximately 2.99°) of the sinusoidal water/sediment interface is smaller than the maximum slope value of 12.1° characterizing test case B. Hence, the horizontal refraction effects are here more gradual than for test case B.

Unlike test cases A, B, a zero-slope bathymetry leads to only two propagating modes. Indeed, recall that the waveguide along the $\theta = 90°$ azimuthal direction is shallower than for test cases A, B. The third mode is more leaky, and thus more rapidly attenuated though still discernable at $t = 5.2$ s in Fig. 7 but completely absent from the next two snapshots ($t = 13.3$ s and $t = 23.4$ s) displayed in the same figure. Looking now at Fig. 8, we observe that, at $t = 3.2$ s, the signal can be decomposed mainly in arrivals of mode 1 and mode 2, though one can notice the (very weak) presence of mode 3. Looking at the next snapshot ($t = 5.2$ s), we observe that

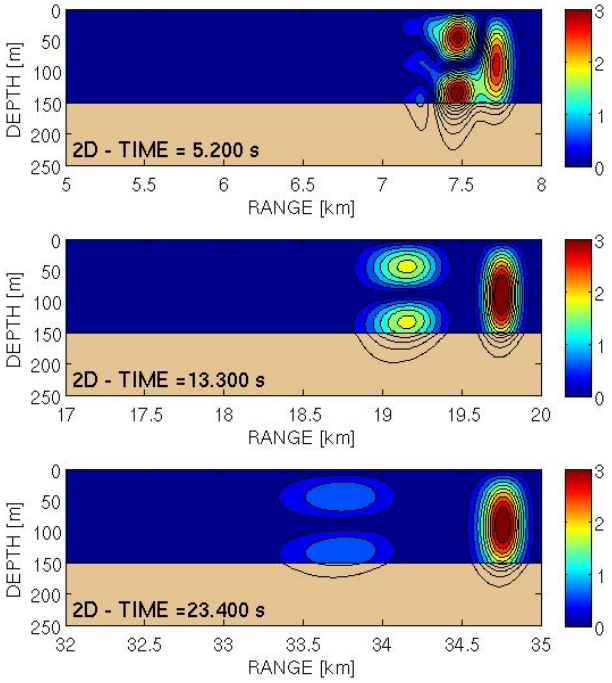

Figure 7: Snapshot of the envelop of the propagating pulse along the $\theta = 90°$ azimuthal direction for test case C corresponding to 2-D PE computations.

mode 3 has disappeared. The cutoff of mode 3 is due to out-of-plane propagation. We also observe that mode 2 progressively disappears, leading to only one propagating mode at $t = 13.3$ s and $t = 16$ s. The snapshots at $t = 20$ s and $t = 23.4$ s exhibit four distinct wave packets. The first one, which is well separated from the three others, corresponds to mode 1. Due to out-of-plane propagation, this first wave packet is accordingly different (*i.e.* weaker and later) from the corresponding 2-D first wave packet. The second and third wave packets correspond to two distincts (but very close) mode-2 arrivals. The fourth packet corresponds to mode 3, with an amplitude of the same order as that of mode 1.

References

[1] A. Tolstoy, "3D propagation issues and models", *J. Comput. Acoust.* **4**, 243–271 (1996).

[2] Movies are accessible at the following url `http://acoustique.ec-lyon.fr/`.

[3] J. Fawcett, "Modeling three-dimensional propagation in an oceanic wedge using parabolic equation methods", *J. Acoust. Soc. Am.* **93**, 2627–2632 (1993).

[4] K. Smith, "A three-dimensional propagation algorithm using finite azimuthal aperture", *J. Acoust. Soc. Am.* **106**, 3231–3239 (1999).

[5] A. Tolstoy, K. Smith, N. Maltsev, "The SWAM'99 workshop - An overview", *J. Comput. Acoust.* **9**, 1–16 (2001).

[6] M. D. Collins, S. A. Chin-Bing, "A three-dimensional parabolic equation model that includes

the effects of rough boundaries", *J. Acoust. Soc. Am.* **87**, 1104–1109 (1990).

[7] F. Sturm, "Numerical simulations with 3DWAPE considering shallow water range-dependent environments", *J. Acoust. Soc. Am.* **109**, 2334–2335 (2001).

[8] S. A. Glegg, G. B. Deane, I. G. House, "Comparison between theory and model scale measurements of the three-dimensional sound propagation in a shear suporting penetrable wedge", *J. Acoust. Soc. Am.* **94**, 2334–2342 (1993).

[9] F. Sturm, "Numerical study of broadband sound pulse propagation in three-dimensional oceanic waveguides", *J. Acoust. Soc. Am.* **117**, 1058–1079 (2005)

[10] F. Sturm, "Computation of broadband sound signal propagation in a shallow water environment with sinusoidal bottom using a 3-D PE model", *Acta Acustica united with Acustica* **93**, 899–908 (2007)

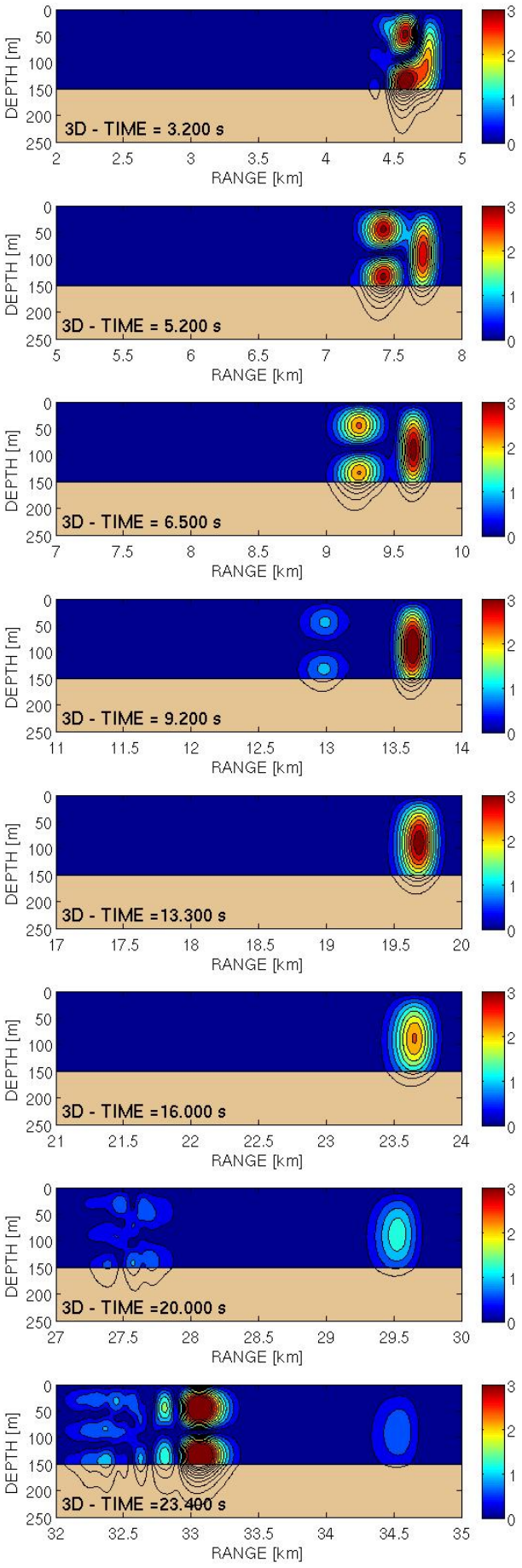

Figure 8: Snapshots of the envelop of the propagating pulse along the $\theta = 90°$ azimuthal direction for test case C corresponding to fully 3-D PE computations.